

# Convection-induced enhancement of mass transfer through an interface separating two immiscible liquids in a two-layer horizontal annulus

A. Yu. Gelfgat<sup>a)</sup>

*Department of Fluid Mechanics and Heat Transfer, Faculty of Engineering, Tel-Aviv University, Ramat Aviv 69978, Israel*

A. L. Yarin and P. Z. Bar-Yoseph

*Faculty of Mechanical Engineering, Technion-Israel Institute of Technology, Haifa 32000, Israel*

(Received 11 March 2002; accepted 19 December 2002; published 4 February 2003)

Two-fluid natural-convection flow in the horizontal cylindrical annulus and its effect on mass transfer through the liquid-liquid interface of two immiscible fluids are studied numerically. The liquids are stratified by gravity, with the denser one occupying the lower part of the annulus. The convective motion is driven by heating of the inner or outer cylindrical boundary. It is shown that the mass transfer of a passive scalar (say, a protein) through the interface can be significantly enhanced by the convective flow. Varying the radii ratio from 0.1 to 0.5, it is found that the mass transfer is more intensive in annuli with smaller radii ratio. No significant difference in the mass transfer rates was found between the heating of either inner or outer cylinder. A possibility of further mass transfer enhancement using more complicated temperature distribution on the boundaries is demonstrated. The problem is related to the search for novel bioseparator devices. © 2003 American Institute of Physics. [DOI: 10.1063/1.1545081]

## I. INTRODUCTION

This work studies the effect of a vortical natural-convection flow on mass transfer through the interface separating two immiscible liquids. The study is motivated by the problem of extraction of admixtures with extremely low diffusion coefficients, e.g., proteins. The purely diffusional mass transfer of such admixtures is too slow and has to be enhanced. A natural way to achieve this goal is recourse to secondary vortical flows.<sup>1</sup> In such flows secondary vortices enhance admixture supply to the interface, which results in steeper concentration gradients there. The latter leads to higher mass fluxes through the interface, even though the diffusion coefficient remains low. In a recently designed bioseparator/bioreactor<sup>2</sup> Taylor–Couette vortical flow is used to enhance the mass transfer. This enhancement was further studied theoretically and numerically in Ref. 3, where the effect of the Taylor vortices and of the axial through flow on the mass transfer rates was investigated. The main disadvantage of the Taylor–Couette apparatus is the contact of rapidly rotating cylindrical boundaries (e.g., in experiments<sup>2</sup> the rotation rate exceeded 10 rev/s) with stationary closed ends, which leads to instability of the liquid-liquid interface. Therefore, it is important to distinguish flows where secondary vortical cells in a two-fluid system can be generated without any mechanical motion of the boundaries. Two such flows were already studied in relation to novel bioseparators/bioreactors: stationary d.c. streaming generated in emulsions<sup>4</sup> and Dean vortices in two-layer systems.<sup>5</sup>

In the present work, in the same context, we are dealing with vortices driven by natural convection in a horizontal

cylindrical annulus filled with equal volumes of two immiscible liquids. The liquid-liquid interface coincides with the horizontal symmetry plane of the annulus; the denser liquid occupies the lower half. It is assumed that the upper liquid contains an admixture (a passive scalar, say, a protein) which diffuses into the lower liquid. When one of the cylindrical boundaries is heated, both liquids are necessarily subjected to a convective motion, which supplies the admixture to the interface. We study the enhancement of the mass transfer by this convection flow for a range of Grashof numbers and radii ratios of the annulus.

Convective flows in a single-layer horizontal cylindrical annulus were intensively studied in relation to nuclear reactor design, cooling of electronic equipment, aircraft cabin insulation, and thermal storage systems (see Refs. 6–9 and references therein). In particular, an analytical solution was found for the velocity field in the case of low Grashof (or Rayleigh) numbers in Ref. 6. Later, such flows were studied as a model yielding a series of different bifurcations.<sup>10–12</sup> When the Grashof number is increased transitions to chaos<sup>13,14</sup> and to turbulence<sup>15,16</sup> take place. To the best of our knowledge, convection in a two-fluid system filling an annulus has never been studied. The mass transfer in horizontal cylindrical annuli was studied in relation to the double diffusion problems and still only in single-fluid cases.<sup>17,18</sup> In the present work novel results for two-fluid systems are discussed. In particular, convective flow patterns and quantitative results on convection-enhanced mass transfer through the liquid-liquid interface are presented.

Section II formulates the problem and briefly discusses the numerical technique used. The results are presented and discussed in Sec. III. Conclusions are drawn in Sec. IV.

<sup>a)</sup>Electronic mail: gelfgat@eng.technion.ac.il

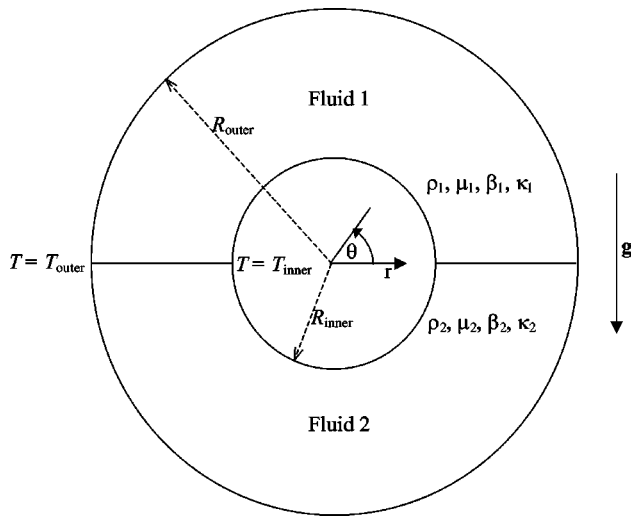


FIG. 1. Sketch of the problem.

**II. FORMULATION OF THE PROBLEM AND NUMERICAL TECHNIQUE**

Consider natural-convection flow in a two-layer horizontal cylindrical annulus, in conjunction with mass transfer through a nondeformable liquid-liquid interface. The system is shown schematically in Fig. 1. The upper and lower halves of the cylinder are filled with two immiscible liquids, denoted fluid 1 and fluid 2. The inner and the outer cylinders are maintained at constant and different temperatures,  $T_{inner}$  and  $T_{outer}$ , respectively. It is assumed that the nondeformable liquid-liquid interface is located at the plane  $\theta = 0, \pi$ , and the mass transfer is assumed not to affect the flow. Denoting all variables and parameters related to the upper and lower halves by subscripts 1 and 2, respectively, the flow in each layer is described by the dimensionless Boussinesq equations

$$\frac{\partial \mathbf{v}_1}{\partial t} + (\mathbf{v}_1 \cdot \nabla) \mathbf{v}_1 = -\nabla p_1 + \Delta \mathbf{v}_1 + Gr T_1, \tag{1}$$

$$\nabla \cdot \mathbf{v}_1 = 0, \tag{2}$$

$$\frac{\partial \mathbf{v}_2}{\partial t} + (\mathbf{v}_2 \cdot \nabla) \mathbf{v}_2 = -\frac{1}{\rho_{21}} \nabla p_2 + \frac{\mu_{21}}{\rho_{21}} \Delta \mathbf{v}_2 + \beta_{21} Gr T_2, \tag{3}$$

$$\nabla \cdot \mathbf{v}_2 = 0, \tag{4}$$

$$\frac{\partial T_1}{\partial t} + (\mathbf{v}_1 \cdot \nabla) T_1 = \frac{1}{Pr} \Delta T_1, \tag{5}$$

$$\frac{\partial T_2}{\partial t} + (\mathbf{v}_2 \cdot \nabla) T_2 = \frac{\lambda_{21}}{c_{21} \rho_{21}} \frac{1}{Pr} \Delta T_2. \tag{6}$$

Here  $\mathbf{v}_k$  is the flow velocity,  $p_k$  is the pressure, and  $T_k$  is the temperature ( $k = 1, 2$ ). Furthermore,  $\rho_{21} = \rho_2 / \rho_1$ ,  $\mu_{21} = \mu_2 / \mu_1$ ,  $\lambda_{21} = \lambda_2 / \lambda_1$ ,  $c_{21} = c_{p,2} / c_{p,1}$ , and  $\beta_{21} = \beta_2 / \beta_1$  are the ratios of the densities, dynamic viscosities, thermal conductivities, heat capacities, and thermal expansion coefficients, respectively,  $Gr = g \beta_1 |T_{inner} - T_{outer}| R_{outer}^3 \rho_1^2 / \mu_1^2$  is the Grashof number and  $Pr = c_{p,1} \mu_1 / \lambda_1 = \nu_1 / \kappa_1$  is the Prandtl number;  $\nu_1$  and  $\nu_2$ ,  $\kappa_1$  and  $\kappa_2$  are the kinematic viscosities and thermal diffusivities of fluids 1 and 2, respectively. The

length, time, velocity and pressure in (1)–(6) are rendered dimensionless by  $R_{outer}$ ,  $R_{outer}^2 \rho_1 / \mu_1$ ,  $\mu_1 / R_{outer} \rho_1$ , and  $(\mu_1 / R_{outer})^2 / \rho_1$ , respectively. The excess dimensionless temperature is  $(T - T_{min}) / (T_{max} - T_{min})$ , where  $T_{min} = \min(T_{inner}, T_{outer})$ , and  $T_{max} = \max(T_{inner}, T_{outer})$ . The excess dimensionless temperature is also denoted by  $T$ . An additional governing parameter describing the problem geometry is the radii ratio  $R_i = R_{inner} / R_{outer}$ . Since we intend to study changes in the transient mass transfer with the variation of the radii ratio  $R_i$ , we choose the length scale as  $R_{outer}$ . This allows the gap width  $d = R_{outer} - R_{inner}$  variation with the inner radius  $R_{inner}$ , keeping the time scale  $R_{outer}^2 \rho_1 / \mu_1$  unchanged. Note that our choice of the length scale corresponds to the one of Refs. 10, 12, and 15 and differs from those used in Refs. 11, 13, 14, and 16–18 where the length scale was  $d$ .

The problem is treated in the polar coordinates  $(r, \theta)$ , in the domain  $R_i \leq r \leq R_o = 1$ ,  $0 \leq \theta \leq 2\pi$ . No-slip boundary conditions are imposed on the cylindrical boundaries

$$r = R_i \text{ or } R_o, \quad \mathbf{v} = 0, \tag{7}$$

and continuity of the velocities, temperature, tangent stresses and heat fluxes is required at the nondeformable liquid-liquid interface  $\theta = 0$  or  $\pi$ :

$$u_1 = u_2, \quad v_1 = v_2 = 0, \tag{8}$$

$$T_1 = T_2, \tag{9}$$

$$\frac{\partial u_1}{\partial \theta} = \mu_{21} \frac{\partial u_2}{\partial \theta}, \tag{10}$$

$$\frac{\partial T_1}{\partial \theta} = \lambda_{21} \frac{\partial T_2}{\partial \theta}. \tag{11}$$

The radial and azimuthal velocity components are denoted by  $u_k$  and  $v_k$ , respectively. The thermal boundary conditions on the cylindrical boundaries are formulated separately according to the inner or outer cylinder is hotter. For the hotter inner cylinder,

$$r = R_i, \quad T = 1; \quad r = R_o, \quad T = 0; \tag{12}$$

and for the hotter outer cylinder

$$r = R_i, \quad T = 0; \quad r = R_o, \quad T = 1. \tag{13}$$

With the steady-state flow calculated, the mass transfer problem is considered. Here we assume that the time needed to reach the convective steady state is much shorter than the characteristic diffusion time, so that the mass transfer during the transient stage is negligible. The mass transfer equations are

$$\frac{\partial c_1}{\partial t} + (\mathbf{v}_1 \cdot \nabla) c_1 = \frac{1}{Sc} \Delta c_1, \tag{14}$$

$$\frac{\partial c_2}{\partial t} + (\mathbf{v}_2 \cdot \nabla) c_2 = \frac{D_{21}}{Sc} \Delta c_2, \tag{15}$$

where  $c_k$ ,  $k = 1, 2$ , are the concentrations of a passive scalar in the fluid layers 1 and 2,  $D_{21} = D_2 / D_1 = O(1)$  is the diffusion coefficient ratio, and  $Sc = \nu_1 / D_1$  is the Schmidt number. The excess dimensionless concentration is  $(c - c_{min}) / (c_{max}$

$-c_{\min}$ ), where  $c_{\max}$  and  $c_{\min}$  are the maximal and minimal concentration values at  $t=0$ , with the upper fluid assumed to contain a uniformly distributed admixture, which begins to diffuse into the lower fluid. Here and hereinafter the excess dimensionless concentration is also denoted by  $c$ . The cylinders are impenetrable for the admixture, and the concentrations and mass fluxes are continuous at the interface. The boundary and initial conditions for the mass transfer problem then read

$$r=R_i \text{ or } R_o, \quad \frac{\partial c}{\partial r}=0, \quad (16)$$

$$\theta=0 \text{ or } \pi, \quad c_1=c_2, \quad \frac{\partial c_1}{\partial \theta}=D_{21} \frac{\partial c_2}{\partial \theta}, \quad (17)$$

$$t=0, \quad c_1=1, \quad c_2=0. \quad (18)$$

For characterization of the mass transfer we introduce the local Sherwood number

$$\text{Sh}(x)=\frac{1}{r} \left. \frac{\partial c}{\partial \theta} \right|_{\theta=0,\pi}, \quad x=r \cos(\theta), \quad (19)$$

and the mass fraction that has diffused into the lower fluid layer

$$m_f=\frac{2}{\pi(1-R_i^2)} \int_{\pi}^{2\pi} \int_{R_i}^1 r c_2(r, \theta) dr d\theta. \quad (20)$$

In the two-layer case the flow problem cannot be solved analytically even in the simplest case of low Grashof numbers, and a numerical calculation is called for. The problems (1)–(12) or (13), and (14)–(18) are solved numerically for  $\text{Gr} \leq 10^5$ . The finite volume method is used with the SIMPLE velocity-pressure decoupling algorithm and semi-implicit three-level time integration scheme. (It was used in Refs. 19 and 20 for swirling flows in cylindrical container and in Ref. 3 for study of the mass transfer enhancement by Taylor vortices. The code was validated additionally for single-fluid convection in a horizontal annulus against the analytical results of Ref. 6 and the numerical results of Ref. 9.) The steady-state fluid flow can be calculated with a dimensionless time step  $\tau=0.1$  for  $\text{Gr} \leq 10^2$ , and with  $\tau=0.01$  for  $10^2 \leq \text{Gr} \leq 10^5$  (usually, several thousands of time steps are necessary to reach a converged solution). For larger Grashof numbers the convective flow becomes oscillatory unstable. Such instability was observed experimentally and numerically in Refs. 12 and 14; its onset can be followed by appearance of multiple flow states<sup>10,11</sup> and by transition to chaos,<sup>12,14</sup> or to three-dimensional flow,<sup>12</sup> all of which are beyond the scope of the present study.

To ensure numerical stability of the mass transfer calculations at large Schmidt numbers characteristic of proteins [ $\text{Sc} \sim \mathcal{O}(10^3)$ ], the calculations are performed with a smaller time step  $\tau=10^{-3}$ . The reported flow and mass transfer calculations are done on the same uniform staggered grid. Jumps in the fluids' physical properties over the liquid-liquid interface were smoothed as in Ref. 3. To ensure mesh- and time-step independence of the results, the calculations for the largest value of the Schmidt number  $\text{Sc}=10^3$  were repeated

on  $100 \times 200$  and  $150 \times 300$  grids in the  $r$ - and  $\theta$ -directions, respectively, with  $\tau=10^{-3}$  and  $10^{-4}$ . No significant changes were found. Most of the mass transfer results reported below refer to the  $100 \times 200$  grid and  $\tau=10^{-3}$ .

Following Ref. 21 we define the viscous, averaging and diffusion time as  $T_e=\rho_1 R_{\text{outer}}^2/\mu_1$ ,  $T_a=T_d \text{Pe}^{-2/3}$ , and  $T_d=R_{\text{outer}}^2/D_1$ , respectively. Here  $\text{Pe}=UR_{\text{outer}}/D_1$  is the Peclet number ( $U$  is a characteristic velocity scale), which can be estimated as  $\text{Pe}=\text{ScGr}$  at small Grashof numbers (i.e., the characteristic velocity proportional to the Grashof number) and  $\text{Pe}=\text{ScGr}^{1/2}$  at large Grashof numbers. It is shown below that for  $\text{Gr} > 10^4$  the fluid velocity increases proportionally to  $\text{Gr}^{1/2}$ . Using the time scale  $R_{\text{outer}}^2 \rho_1/\mu_1$ , we obtain the following dimensionless values:  $T_e=1$ ,  $T_a=\text{Sc}^{1/3} \text{Gr}^{-2/3}$ ,  $T_d=\text{Sc}$  at small Grashof numbers, while  $T_a=\text{Sc}^{1/3} \text{Gr}^{-1/3}$  at large Grashof numbers with  $T_e$  and  $T_d$  the same as for the small Grashof numbers. In the calculations reported below  $\text{Sc}=10^3$ , and  $1 \leq \text{Gr} \leq 10^5$ , so that  $T_a \leq 10$ ,  $T_d=10^3$  at small Grashof numbers ( $1 \leq \text{Gr} \leq 100$ ), whereas  $T_a \ll 1$  and  $T_d=10^3$  at large Grashof numbers ( $\text{Gr} \geq 10^4$ ). The range of integration over time for the mass transfer problem was 100, so that it was always longer than the viscous and the averaging time and shorter than the diffusion time. The physical meaning of the time scales is the following. The viscous time  $T_e$  represents the time scale characterizing transition to the steady state convection. The diffusion time  $T_d (\gg T_e)$  characterizes the duration of full mixing of the admixture by pure diffusion. When the averaging time  $T_a$  is intermediate between  $T_e$  and  $T_d$ , as in the case  $1 \leq \text{Gr} \leq 100$ , it yields the time scale of the mass transfer process enhanced by the vortical flow. On the other hand, at the higher values of  $\text{Gr}$  the time scale  $T_a$  becomes as small as the viscous time and does not represent the rate of the mass transfer process.

### III. RESULTS AND DISCUSSION

In the calculations the Grashof number  $\text{Gr}$  was varied from 1 to  $10^5$  and the radii ratio  $R_i$  from 0.1 to 0.5. The other governing parameters were fixed. Since we were mostly interested in the protein solutions studied experimentally in Ref. 1, we chose  $\text{Pr}=7$  and  $\text{Sc}=10^3$ , which is characteristic of water and protein solutions. The density and viscosity ratios were taken from the experiments as  $\rho_{21}=1.4$  and  $\mu_{21}=0.96$ , respectively. Since the thermophysical properties of the two protein solutions should be close, and taking into account the differences of the experimental liquids used in Ref. 1, we chose the values of the other parameter ratios close to unity, namely  $c_{21}=1.2$ ,  $\beta_{21}=1.3$ , and  $D_{21}=1.5$ .

#### A. Flow patterns

The maximal value of the stream function calculated numerically for a test case of a single-layer fluid in the annulus was compared to the analytical solution at the Stokes limit for small values of the Grashof (or Rayleigh) number similar to that of Ref. 6. The calculations were performed on a uniform grid with  $50 \times 100$  nodes in the  $r$ - and  $z$ -directions, respectively. At small Grashof numbers the numerical and analytical solutions coincide up to the fourth decimal digit.

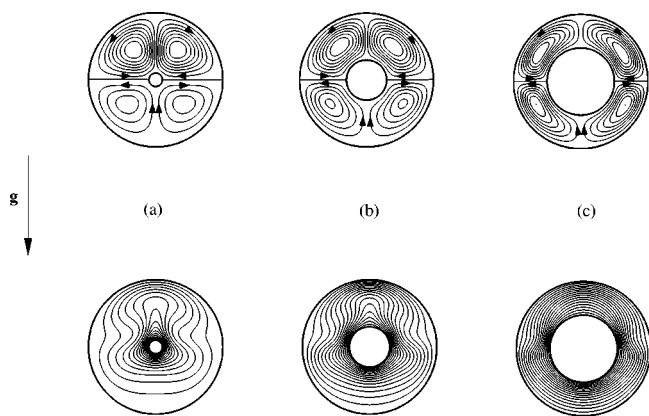


FIG. 2. Streamlines (upper frames; here and hereafter  $\psi$  denotes stream function) and isotherms (lower frames) of the convective flow at  $Gr=10^3$ . Inner cylinder heated, outer cooled. (a)  $R_i=0.1$ ,  $|\psi|_{\max}^{(1)}=0.500$ ,  $|\psi|_{\max}^{(2)}=0.205$ , (b)  $R_i=0.3$ ,  $|\psi|_{\max}^{(1)}=0.402$ ,  $|\psi|_{\max}^{(2)}=0.253$ , and (c)  $R_i=0.5$ ,  $|\psi|_{\max}^{(1)}=0.203$ ,  $|\psi|_{\max}^{(2)}=0.176$ .

The two solutions begin to diverge at  $Gr \approx 100$ , beyond which the influence of the nonlinear terms becomes significant. The calculated flow patterns in the two-layer case are plotted in Figs. 2–5; superscripts 1 and 2 refer to the fluids in the upper and lower layers 1 and 2, respectively. The direction of the flows is indicated by arrows. Obviously, when the inner cylinder is heated (Figs. 2 and 3) the fluids ascend along it and descend along the outer cylinder. The direction of the convective cells is reversed when the outer cylinder is heated (Figs. 4 and 5). Note that in the cases when the inner cylinder is hotter, the upper fluid is unstably stratified (i.e., the hotter fluid is below), and the lower fluid stably stratified (i.e., the hotter fluid is above). Therefore, the convective motion in the upper fluid is more intensive. This effect reverses when the outer cylinder is hotter. Then the upper fluid is stably stratified and the lower one—unstably, which leads to more intensive convective motion in the lower fluid. Note also that in the developed nonlinear regime the maximal values of the stream function  $\psi$  in the more intensive vortical

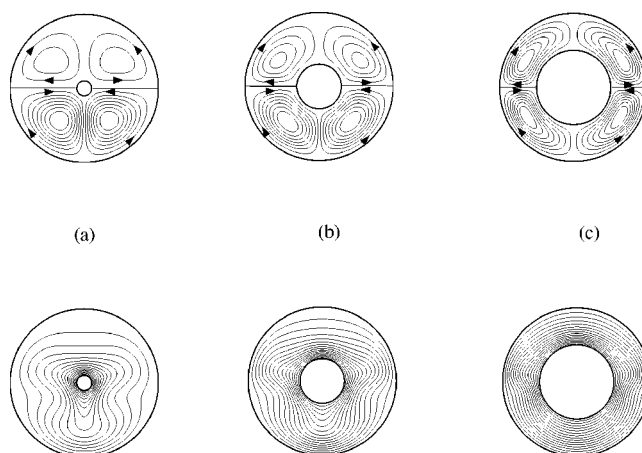


FIG. 4. Streamlines (upper frames) and isotherms (lower frames) of the convective flow at  $Gr=10^3$ . Outer cylinder heated, inner cooled. (a)  $R_i=0.1$ ,  $|\psi|_{\max}^{(2)}=0.561$ ,  $|\psi|_{\max}^{(1)}=0.166$ , (b)  $R_i=0.3$ ,  $|\psi|_{\max}^{(2)}=0.417$ ,  $|\psi|_{\max}^{(1)}=0.219$ , and (c)  $R_i=0.5$ ,  $|\psi|_{\max}^{(2)}=0.198$ ,  $|\psi|_{\max}^{(1)}=0.170$ .

cells are larger when the outer cylinder is hotter, compared with the other case of the hotter inner cylinder. Conversely, the maximal values of the stream function in the less intensive vortical cells are larger when the inner cylinder is hotter, compared with the other case of the hotter outer cylinder (cf. Figs. 2 and 4; Figs. 3 and 5). When the convection of heat is not emphasized strongly the intensity of the vorticities is close in both cases [cf. Figs. 2(c) and 4(c)]. Larger values of the stream functions mean stronger mixing by the vortical flow. Therefore, one can expect the mass transfer through the liquid-liquid interface to differ according to which cylinder is heated.

The considered values of the Grashof number  $Gr=10^3$  and  $10^4$  correspond, for example, to aqueous solutions with the temperature difference  $|T_{\text{outer}} - T_{\text{inner}}| = 1.25$  and  $12.5$  K in the case of  $R_{\text{outer}} = 2$  cm,  $R_{\text{inner}} = 1$  cm,  $\beta_1 = 5 \times 10^{-5} \text{ K}^{-1}$  and  $\nu_1 = 10^{-2} \text{ cm}^2/\text{s}$ . For example, for  $Gr = 5 \times 10^3$  and  $|T_{\text{outer}} - T_{\text{inner}}| = 1.25$  K the maximal flow velocities are  $u_{\max} = 0.028$  cm/s and  $v_{\max} = 0.035$  cm/s for the ra-

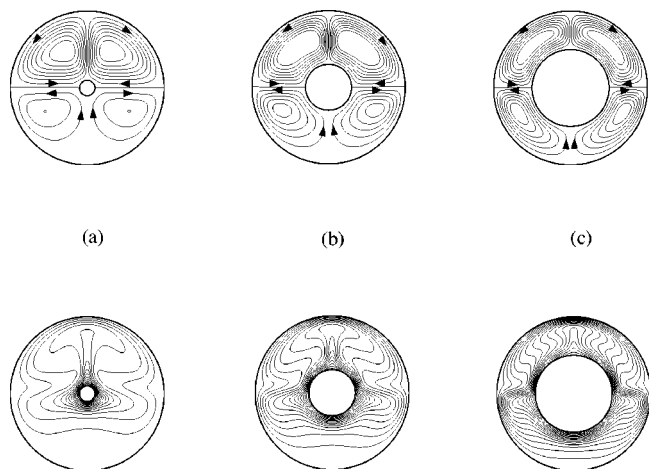


FIG. 3. Streamlines (upper frames) and isotherms (lower frames) of the convective flow at  $Gr=10^4$ . Inner cylinder heated, outer cooled. (a)  $R_i=0.1$ ,  $|\psi|_{\max}^{(1)}=1.705$ ,  $|\psi|_{\max}^{(2)}=0.568$ , (b)  $R_i=0.3$ ,  $|\psi|_{\max}^{(1)}=1.453$ ,  $|\psi|_{\max}^{(2)}=0.848$ , and (c)  $R_i=0.5$ ,  $|\psi|_{\max}^{(1)}=1.082$ ,  $|\psi|_{\max}^{(2)}=0.920$ .

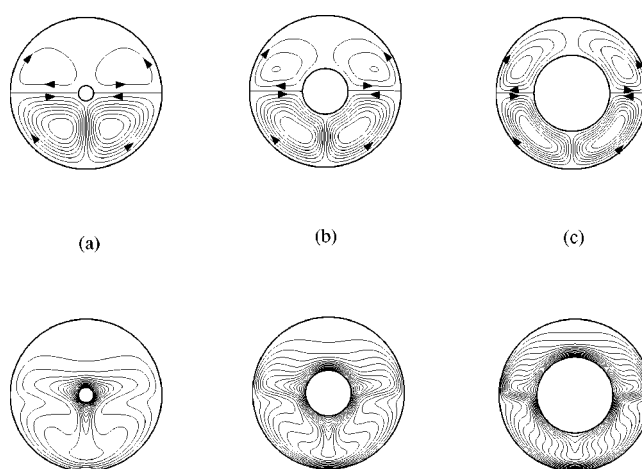


FIG. 5. Streamlines (upper frames) and isotherms (lower frames) of the convective flow at  $Gr=10^4$ . Outer cylinder heated, inner cooled. (a)  $R_i=0.1$ ,  $|\psi|_{\max}^{(2)}=2.140$ ,  $|\psi|_{\max}^{(1)}=0.409$ , (b)  $R_i=0.3$ ,  $|\psi|_{\max}^{(2)}=1.818$ ,  $|\psi|_{\max}^{(1)}=0.617$ , and (c)  $R_i=0.5$ ,  $|\psi|_{\max}^{(2)}=1.291$ ,  $|\psi|_{\max}^{(1)}=0.731$ .

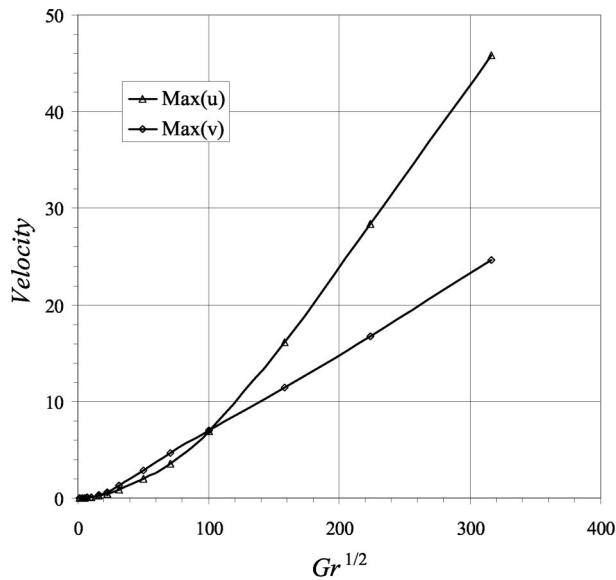


FIG. 6. Scaling of the maximal velocity components with  $Gr^{1/2}$  for  $R_i = 0.5$ .

dial and azimuthal velocity components, respectively. By contrast, for  $Gr = 5 \times 10^4$  and  $|T_{\text{outer}} - T_{\text{inner}}| = 12.5$  K,  $u_{\text{max}} = 0.18$  cm/s and  $v_{\text{max}} = 0.13$  cm/s. For comparison, in Ref. 3 the secondary flow velocity in a two-layer Taylor–Couette apparatus was found to be of the order of 0.6 cm/s under realistic conditions.

In novel bioseparators based on the Dean vortices in coiled pipes the maximal secondary transverse velocity as high as 2.8 cm/s can be achieved.<sup>22</sup> Therefore the secondary flow in the present variant of a novel bioseparator based on natural convection is weaker than in the Taylor–Couette and the Dean counterparts. However, its construction is much simpler: it does not contain any moving parts and is based on the simplest geometry of a straight pipe. Also at higher temperature differences, say at  $|T_{\text{outer}} - T_{\text{inner}}| = 50$  K, much higher secondary flow velocities of the order of 0.35 cm/s can be achieved. Therefore, in the cases when the chemical nature of the admixture allows higher temperature differences, the present device becomes as fast as the Taylor–Couette bioseparator.

For the devices based on secondary dc streaming flows arising due to capillary waves at droplet surfaces in emulsions or at the interface between two liquid layers in a channel,<sup>4,23</sup> the corresponding velocities are of the order of 0.052 and 0.0018 cm/s, respectively. Therefore the present natural-convection-based device can be more effective for mass transfer enhancement. However, in the case of droplets in emulsions<sup>4</sup> a weaker secondary flow can be compensated by a significantly larger interfacial area, which can result in a higher overall mass transfer.

Narrow thermal boundary layers develop near the cylindrical boundaries and the liquid-liquid interface at larger Grashof numbers (Figs. 3 and 5). They always appear near the inner cylinder, and at larger aspect ratio become noticeable also near the outer one [cf. Figs. 3(a) and 3(c); Figs. 5(a)

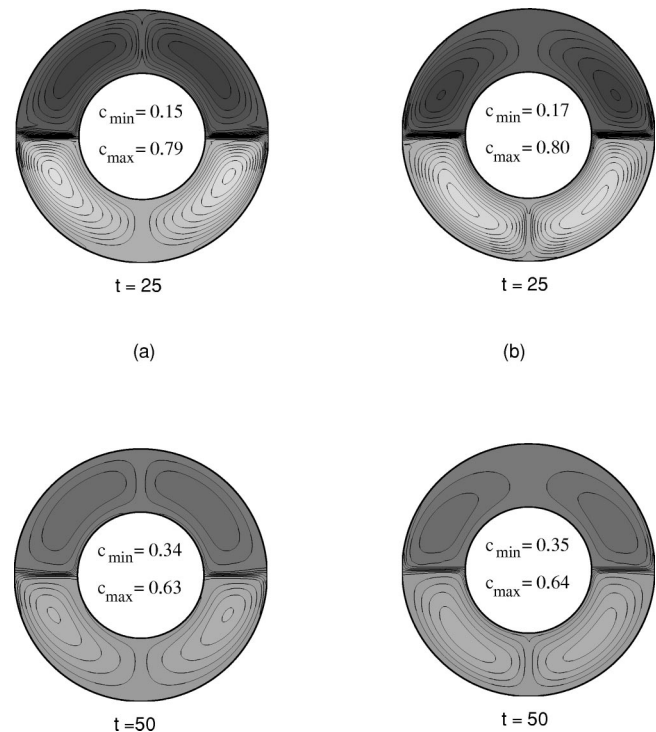


FIG. 7. Instantaneous concentration contours at different time moments. The case of  $R_i = 0.5$ ,  $Gr = 10^4$ , inner cylinder heated. Forty-five concentration contours equally distributed between  $c = 0$  and  $c = 1$ . (a) Inner cylinder heated; (b) outer cylinder heated.

and 5(c)]. Their existence necessitates finer spatial resolution, especially at large Schmidt numbers. As mentioned, most of the calculations were carried out on the uniform grid  $100 \times 200$ , which yields mesh-independent modeling of the mass transfer at  $Sc = 10^3$ . The boundary layers themselves can also be resolved on coarser grids (e.g.,  $75 \times 100$ ).

The important feature of the flow patterns is the direction of fluid motion along the liquid-liquid interface. Note that this motion is opposite on the two sides at some distance from the interface (Figs. 2–5). This is different from the previously considered cases where the mass transfer through the interface is enhanced by cocurrent vortical motion,<sup>1–4</sup> thus, the theoretical considerations and conclusions of these studies are not directly applicable to the present problem. Note also that the countercurrent flow near the interface in the present case could, in principle, make it unstable. However, in the present case gravitational stratification is expected to be a dominant stabilizing factor.

Figure 6 shows how the maximal velocity components scale with  $Gr^{1/2}$ . At small Grashof numbers the velocity increases linearly with  $Gr$  in accordance with the analytical solution,<sup>6</sup> corresponding to the creeping flow case. For the Grashof number above the value of approximately  $10^3$ , the  $Gr^{1/2}$  scaling is clearly seen (Fig. 6). This is usual for natural convective flows and validates the above application of velocity scaling for evaluation of the averaging time  $T_a$  and the Peclet number.

## B. Mass transfer

Calculations of the mass transfer were carried out for a fixed value of the Schmidt number,  $Sc = 10^3$ , and for varying

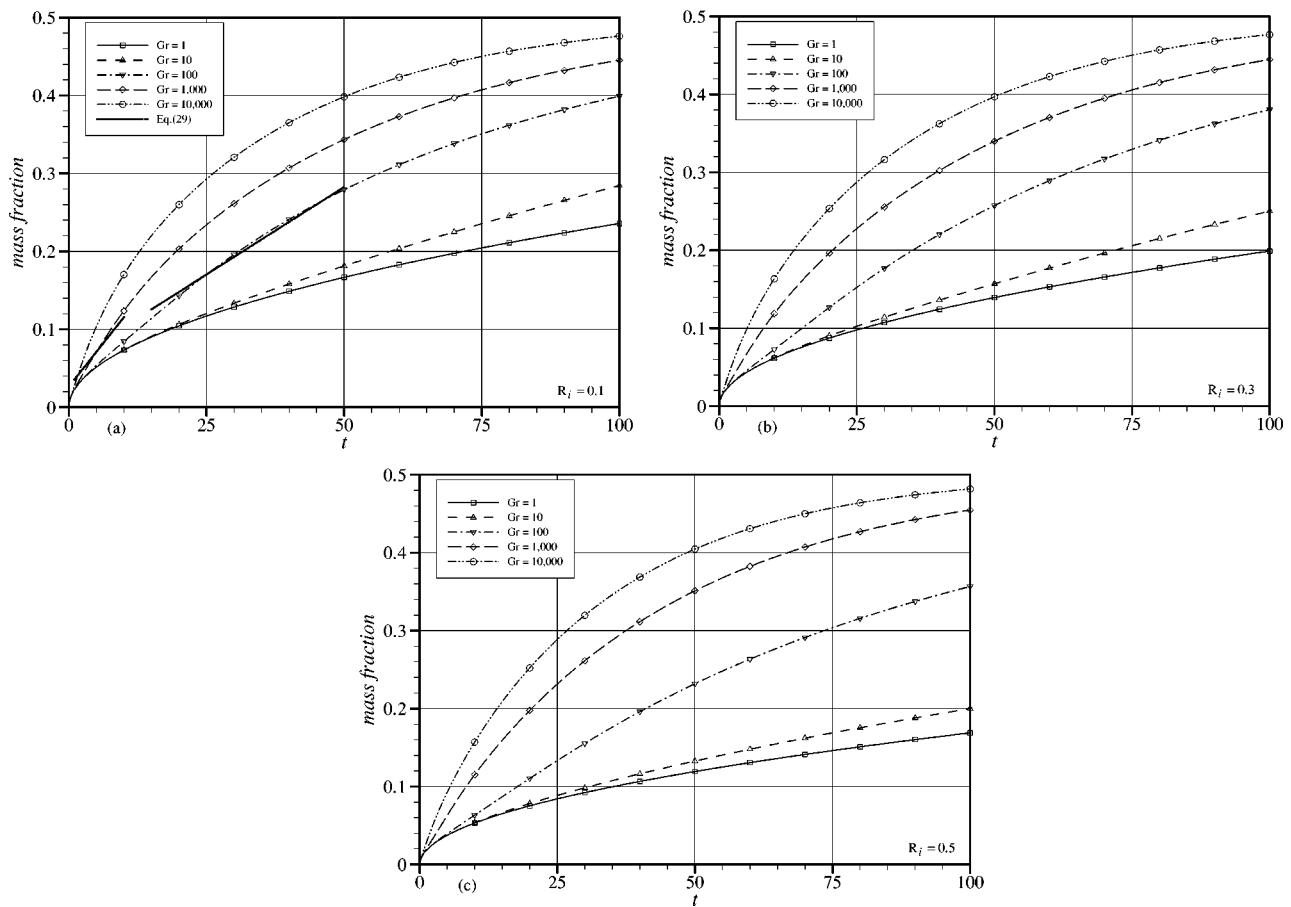


FIG. 8. Time histories of the mass fraction  $m_f$ . Inner cylinder is heated. Dotted lines corresponding to  $Gr=10^2$  and  $10^3$  at  $R_i=0.1$  were obtained using Eq. (29).

Grashof number and radii ratio. Instantaneous snapshots of the concentration field are shown in Figs. 7(a) and 7(b). The maximal and minimal instantaneous values of the concentration are shown in each frame. It is seen that in the case of the heated inner cylinder the mass transfer proceeds at almost the same rate as in the case of the heated outer cylinder. The same is observed in the time histories of the mass fraction  $m_f$  calculated in fluid 2, and depicted in Fig. 8 for the heated inner cylinder. For the case of the heated outer cylinder the dependencies  $m_f(t)$  are almost indistinguishable from those plotted in Fig. 8. However, in the case of the heated inner cylinder the mass transfer always remains slightly faster. Thus, for example, the values of  $m_f$  at  $Gr=10^4$ ,  $R_i=0.1$  and  $t=100$  are 0.476 and 0.470 for the heated inner and heated outer cylinders, respectively. Such a small difference can be attributed to the almost identical physical properties of the liquids chosen for the present simulation. The convective vortices at small Grashof numbers are also almost identical; in the case of the heated inner cylinder the larger vortices appear in the upper layer, and in that of the outer cylinder—in the lower layer. At larger Grashof numbers the flow patterns differ (Figs. 2–5), but the overall mass transfer rate remains almost the same for the two cases. Such a negligible difference in the mass transfer rates allows one to choose which cylinder to heat in accordance with technological feasibility and other restrictions not related to the mass

transfer itself. It is seen that the mass fraction increases monotonically with the Grashof number in all the cases depicted. This means that the mass transfer is intensified by the natural-convection flow, which enhances admixture supply to the interface.

The radii ratio  $R_i$  has a visible effect on the mass transfer rate only at relatively low values of the Grashof number, as Figs. 9 and 10 show. At low Grashof numbers the mass transfer is always more intensive in the annuli with smaller radii ratio  $R_i$  for  $R_i \leq 0.3$  [Fig. 9(a)] and  $R_i \leq 0.5$  [Fig. 10(a)]. However, at larger  $Gr$  the effect is opposite. To explain this we need a better insight into the mechanism of mass transfer enhancement. The direction of flows in Figs. 2 and 3 (inner cylinder heated) shows that the larger concentration in the upper half of the annulus is transported along the outer cylinder towards the interface, and from the outer to the inner cylinder towards the interface itself; the smaller concentration is transported in the lower half of the annulus along the inner cylinder, and from the inner to the outer cylinder along the interface. This means that the convective flow transports fluids with smaller and larger admixture concentrations towards the interface, which increases the concentration gradient normal to the interface. This, in turn, yields a higher mass transfer rate through the interface. The flow directions along the interface show also that a maximum of the normal component of the concentration gradient can be expected at the

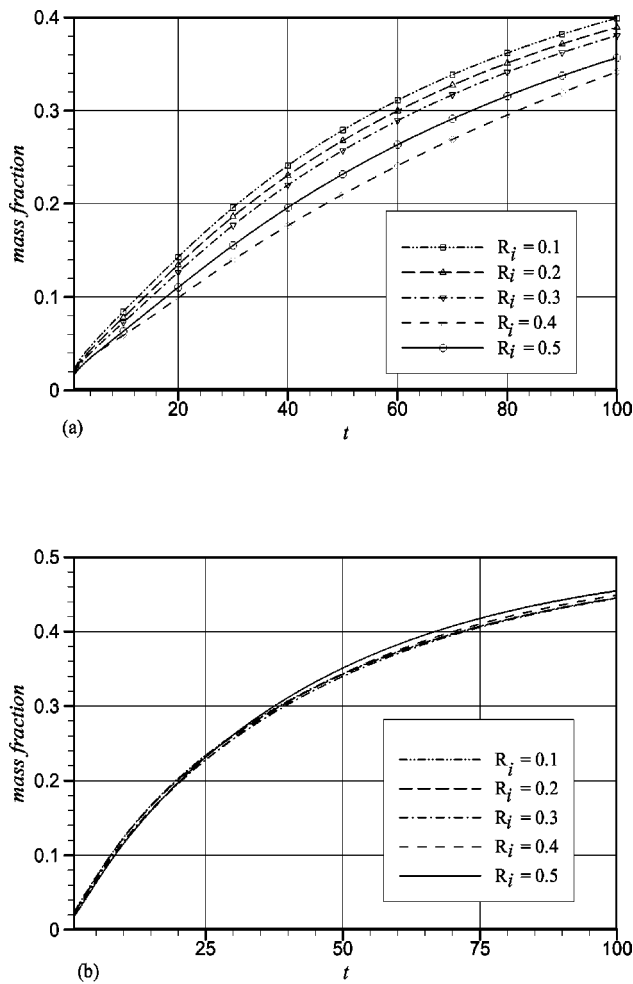


FIG. 9. Time histories of the mass fraction  $m_f$  for different radii ratio; (a)  $Gr=100$ , (b)  $Gr=10^3$ . Inner cylinder heated.

interface somewhere between the cylindrical boundaries, where the highest and the lowest concentrations “meet.” This maximum will be larger for more intensive convective flows, which will lead to the mass transfer enhancement with the growth of  $Gr$ . Another factor affecting the mass transfer rate is the total area of the liquid-liquid interface. It is clear that at smaller radii ratio the area is larger. On the other hand, the temperature gradient driving the flow is roughly estimated as  $(T_{max}-T_{min})/(R_{outer}-R_{inner})$ . With  $R_{outer}$  fixed and  $R_{inner}$  decreasing (then the radii ratio  $R_i$  is also decreasing) the temperature gradient decreases and so does the intensity of the convective flow. Thus, we observe here two competitive mechanisms affecting the mass transfer with the variation of the radii ratio: with the decrease of  $d=R_{outer}-R_{inner}$  the interfacial area increases tending to increase the mass transfer rate; however, the intensity of the convective motion decreases causing the opposite effect. At the parameters considered, the competition of these two mechanisms leads to the following cumulative effects: at lower  $Gr$  small radii ratios ( $R_i=0.1$  for the inner and outer cylinders heated) are preferable for mass transfer enhancement, while at larger  $Gr$  larger radii ratios ( $R_i=0.5$  for the inner and outer cylinders heated) provide a slightly faster mass transfer rate (Figs. 9 and 10).

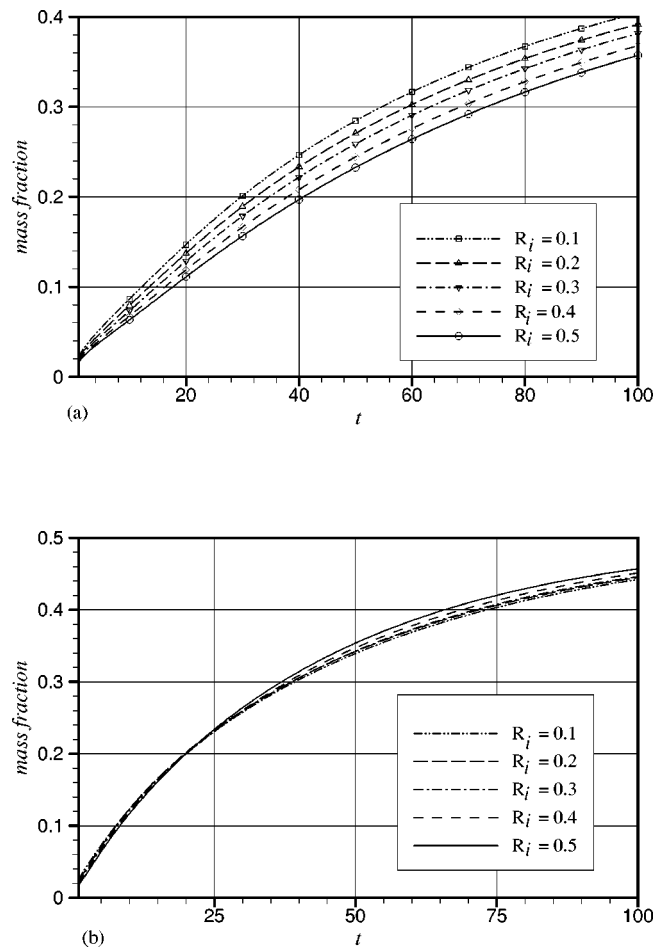


FIG. 10. As Fig. 9, outer cylinder heated.

An additional illustration of the effect of the above-mentioned competitive mechanisms is seen in Fig. 11 depicting the instantaneous profiles of the Sherwood number (19) calculated at  $Gr=10^4$  and different radii ratios. The Sherwood number is plotted for the right-hand side of the interface only. The mass transfer rate at a fixed time is defined by the integral  $\int Sh(r)dr$  taken over the whole interface. With the decrease of the radii ratio  $R_i$  the integral is taken over the larger interval but local values of  $Sh(r)$  are mainly smaller (except for the regions of maximal values) than those corresponding to the larger  $R_i$ .

At two fixed values of time  $t=25$  and  $50$  the diffused mass fraction  $m_f$  scales as  $Gr^\alpha$  with  $\alpha=\frac{1}{4}$  for  $50 < Gr < 10^3$  and  $\alpha \approx \frac{1}{9}$  for  $Gr > 10^4$ .

It is emphasized that as time increases the transient effects disappear and the mass transfer approaches a quasi-stationary state when

$$\overline{\frac{\partial c_k}{\partial t}} \ll \overline{(\mathbf{v} \cdot \nabla) c_k} \tag{21}$$

near the interface. (The overbars denote averaging over a slice with thickness  $\Delta r \times r \Delta \theta \sim d \times 0.2d$  near the interface which is its centerline.) To verify the approach to quasi-steadiness of the mass transfer in the present case we monitored the ratio  $q(t)$  of the averaged time derivative to the averaged convective derivative

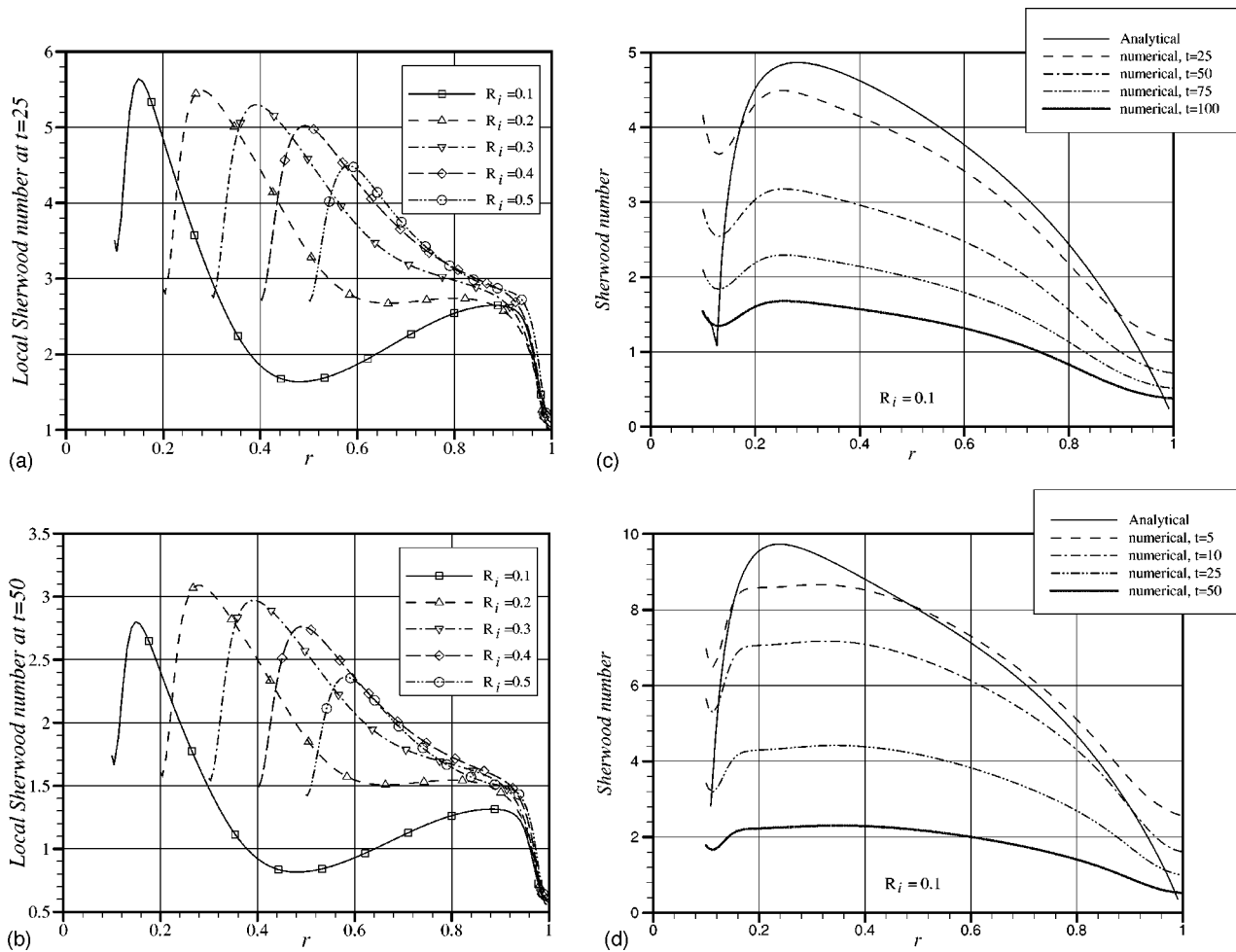


FIG. 11. Instantaneous distributions of the local Sherwood number at the liquid-liquid interface.  $Gr=10^4$ , outer cylinder heated. (a)  $t=25$ ; (b)  $t=50$ ; and (c) comparison of the calculated instantaneous local Sherwood numbers with the one calculated using Eq. (28) for  $Ri=0.1$ ,  $Gr=100$ ; (d) same as (c) for  $Gr=10^3$ .

$$q(t) = \frac{\overline{\partial c_k / \partial t}}{(\mathbf{v} \cdot \nabla) c_k} \tag{22}$$

The result is plotted in Fig. 12. In the case of the inner cylinder heated it is seen that quasi-steadiness (corresponding to, say,  $q < 0.02$ ) is already reached for  $Gr=10^2$  and  $10^3$  ( $Ri=0.1$ ) at any time from the range  $0 \leq t \leq 100$ . On the other hand, approach to quasi-steadiness in the case of the outer cylinder heated is much slower. In this case, for example, for  $Gr=10^4$  and  $Ri=0.1$  the quasi-stationary state cannot be reached at  $t < 100$ .

At the quasi-stationary state an additional insight into the mass transfer in the case of countercurrent flow can be facilitated by the fact that for  $Sc=10^3$  very narrow concentration boundary layers develop near the interface in both fluids. The velocity components along the interface and normal to it in both fluids can then be represented as  $u_k = \gamma_k(X_k)Y_k$  and  $v_k = -(d\gamma_k/dX_k)Y_k^2/2$ . Here  $\gamma_k > 0$  ( $k=1,2$ ) denote the shear rates in the fluids, and the coordinate systems  $X_k, Y_k$  are associated with the interface, with  $X_k$  directed along it and  $Y_k$  normally and into the corresponding liquid layer. It is emphasized that in the numerical calculations  $u_k$  are nonzero at the interface in the general case [cf.

(8)]. However, for the parameter values used  $u_k$  appear to be rather close to zero. Therefore, to construct the boundary layer solution  $u_k$  were approximately taken to be zero at the interface. Note also that  $X_1$  and  $X_2$  have the same origin and  $X_1 = -X_2 + d$ . The concentration distributions in the boundary layers are given by

$$\gamma_k(X_k)Y_k \frac{\partial c_k}{\partial X_k} - \frac{1}{2} \frac{d\gamma_k}{dX_k} Y_k^2 \frac{\partial c_k}{\partial Y_k} = D_k \frac{\partial^2 c_k}{\partial Y_k^2}, \tag{23}$$

$$Y_1 \rightarrow \infty, \quad c_1 = c_{1\infty}, \tag{24}$$

$$Y_2 \rightarrow \infty, \quad c_2 = c_{2\infty}, \tag{25}$$

$$Y_1 = Y_2 = 0, \quad c_1 = c_2, \tag{26a}$$

$$Y_1 = Y_2 = 0, \quad -D_1 \frac{\partial c_1}{\partial Y_1} = D_2 \frac{\partial c_2}{\partial Y_2}. \tag{26b}$$

The solution of problem (23)–(26), generalizing the one found previously for a single-layer case in Ref. 24, permits the calculation of the concentration profiles  $c_i = F_i(Z_i)$  depending in the present case on a single variable

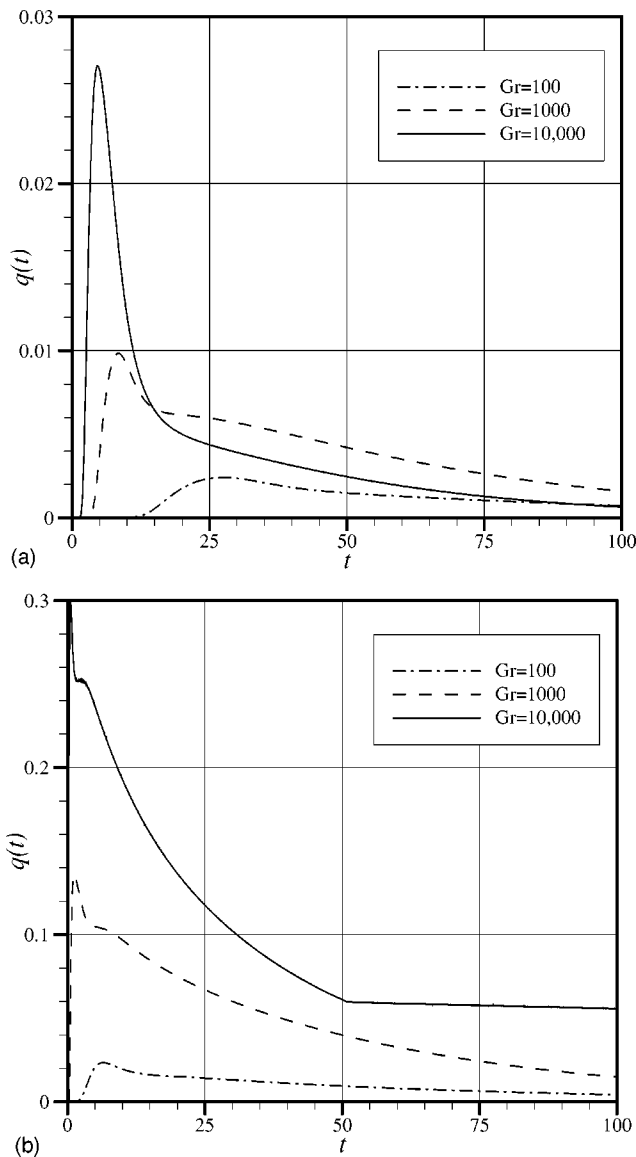


FIG. 12. Time history of the quantity  $q(t)$  showing the ratio of the averaged concentration time derivative to the averaged concentration convective derivative in the slice  $\sim d \times 0.2d$  containing the liquid-liquid interface. Case  $R_i = 0.1$ . (a) Inner cylinder heated; (b) outer cylinder heated.

$$Z_i = \frac{Y_i [\gamma_i(X_i)]^{1/2}}{\left\{ \int_0^{X_i} [\gamma_i(\xi)]^{1/2} d\xi \right\}^{1/3}} \quad (27)$$

The solution we are searching for is subject to the following conditions: near the outer cylinder at  $X_1 = 0$  for any  $Y_1$  the concentration  $c_1 = c_{1\infty}$ , whereas near the inner cylinder at  $X_2 = 0$  for any  $Y_2$  the concentration  $c_2 = c_{2\infty}$ . In the present case of the counterflow near the interface (cf. Figs. 2–5) the “upstream” end of the boundary layer in one phase is the “downstream” end of the other.

The local Sherwood number,  $Sh_m = h_m R_{\text{outer}} / D_1$  ( $h_m$  being the mass transfer coefficient) is then found as

$$Sh_m(X_2) = \frac{Sc^{1/3}}{9^{1/3} \Gamma(\frac{4}{3})} [\gamma_2(X_2)]^{1/2} \times \left[ \left( \frac{D_1}{D_2} \right)^{2/3} \left\{ \int_0^{X_2} [\gamma_2(\xi)]^{1/2} d\xi \right\}^{1/3} + \left[ \frac{\gamma_2(X_2)}{\gamma_1(-X_2 + 1 - R_i)} \right]^{1/2} \times \left\{ \int_0^{-X_2 + 1 - R_i} [\gamma_1(\xi)]^{1/2} d\xi \right\}^{1/3} \right]^{-1}, \quad (28)$$

where  $\Gamma(\cdot)$  denotes the gamma-function and the shear rates are dimensionless, the shear rates are rendered dimensionless by  $\mu_1 / (R_{\text{outer}}^2 \rho_1)$ , and  $X_2$  and  $\xi$  by  $R_{\text{outer}}$ .

The distributions of the local Sherwood number based on the values of  $\gamma_1(x)$  and  $\gamma_2(x)$  found numerically are compared with the numerically obtained instantaneous Sherwood numbers in Figs. 11(c) and 11(d) for the heated inner cylinder. It is seen that Eq. (28) yields the profiles which are fairly close to the numerical ones at  $t \leq t_m$  with  $t_m = 25$  for  $Gr = 100$  and with  $t_m = 5$  for  $Gr = 10^3$  (in both cases  $R_i = 0.1$ ). The comparison of the Sherwood numbers calculated numerically and defined by Eq. (28) for the heated outer cylinder yields similar results.

According to Fig. 12(a) for the heated inner cylinder the above-mentioned time intervals  $t \leq t_m$  already correspond to  $q \ll 1$ , which means that the transient effects in the interfacial mass transfer mechanism are already expected to be relatively small. Therefore we can conclude that the boundary layer approximation considered above yields plausible results. At much higher values of  $t$  the mixing effects throughout the flow region become significant and the boundary conditions (24) and (25) are violated, which makes Eq. (28) invalid irrespective of the fact that the transient effects have disappeared. Bulk mixing is stronger at higher values of  $Gr$ , which is the reason of the lower values of  $t_m$  at higher  $Gr$ .

The distribution of  $Sh_m$  found from (28) using the values of  $\gamma_1(x)$  and  $\gamma_2(x)$  calculated at  $t = t_m$  can be used to approximate the results for the mass fraction  $m_f$  at  $t$  close enough to  $t_m$ . This yields

$$m_f = m_{f,m} + \frac{2}{\rho_{21} Sc} (t - t_m) \int_0^{1-R_i} Sh_m(X_2) dX_2, \quad (29)$$

where  $m_f$  and its value at  $t = t_m$ ,  $m_{f,m}$ , found numerically are rendered dimensionless by  $R_{\text{outer}}^2 \rho_1^2 D_1 / \mu_1$ . The results corresponding to Eq. (29) are shown in Fig. 8 by straight solid lines.

### C. Search for optimal heating conditions

In the previous subsections cylindrical boundaries of the annulus are maintained at constant temperatures. In principle, it is possible to search for more complicated thermal boundary conditions, which can provide a more intensive convective flow and, consequently, a larger mass transfer rate. The corresponding optimization problem is extremely complicated and is far beyond the scope of the present study. In the following we illustrate a possibility to intensify the

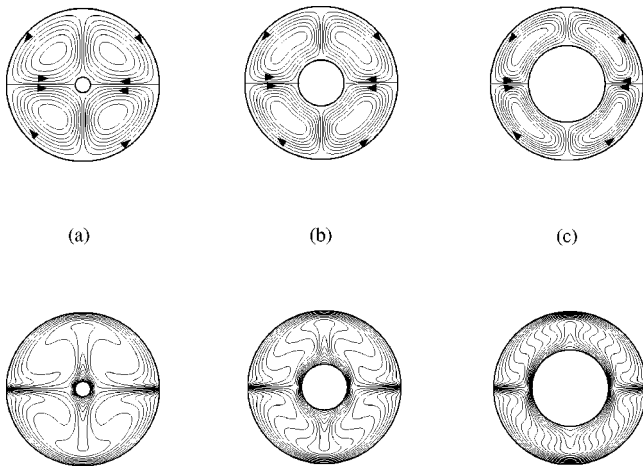


FIG. 13. Streamlines (upper frames) and isotherms (lower frames) of the convective flow at  $Gr=10^4$ . Unstably stratified configuration. (a)  $R_i=0.1$ ,  $|\psi|_{\max}^{(1)}=2.770$ ,  $|\psi|_{\max}^{(2)}=2.211$ , (b)  $R_i=0.3$ ,  $|\psi|_{\max}^{(1)}=1.931$ ,  $|\psi|_{\max}^{(2)}=1.522$ , and (c)  $R_i=0.5$ ,  $|\psi|_{\max}^{(1)}=1.330$ ,  $|\psi|_{\max}^{(2)}=1.107$ .

mass transfer by alteration of the boundary conditions by the following example. We assume that the lower half of the outer cylinder and the upper half of the inner cylinder are heated, while the remaining parts of the boundaries are cooled. This heating creates an unstable density stratification (heating from below) in each liquid, and at the same time retains the same temperature difference in the horizontal direction. Given the fact that the cylinders are typically made of materials with rather large thermal conductivity (e.g., metals), practical feasibility of these nonuniform temperature distributions over the boundaries is rather problematic. Nevertheless, it is worth examining this case as a minimum, as a theoretical opportunity. Therefore the objective of the following is to demonstrate that alteration of the thermal boundary conditions allows an additional mass transfer enhancement.

The boundary conditions (12) and (13) are now replaced by

$$r=R_i, \quad 0 \leq \theta \leq \pi: \quad T=1, \tag{30}$$

$$r=R_i, \quad \pi \leq \theta \leq 2\pi: \quad T=0, \tag{31}$$

$$r=R_o, \quad 0 \leq \theta \leq \pi: \quad T=0, \tag{32}$$

$$r=R_o, \quad \pi \leq \theta \leq 2\pi: \quad T=1. \tag{33}$$

In the following we refer to the problem defined by (1)–(11), (14)–(18), and (30)–(33) as the unstably stratified configuration.

The convective flows calculated for the unstably stratified configuration at  $Gr=10^4$  are depicted in Fig. 13. Comparison of convective flows at  $Gr=10^4$  (cf. Figs. 13, 3 and 5) shows that the unstably stratified configuration yields developed vortices in both fluids, which are as intensive as the main vortices calculated for the heated inner (Fig. 3) or outer (Fig. 5) cylinder. Note that in Figs. 3 and 5 significant vortices developed only in one of the two fluids. Besides that, comparison of the stream function maxima shows that the vortices yielded by the unstably stratified configuration (Fig.

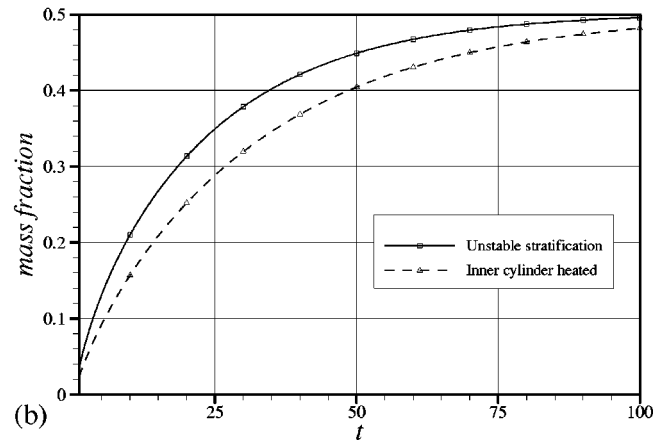
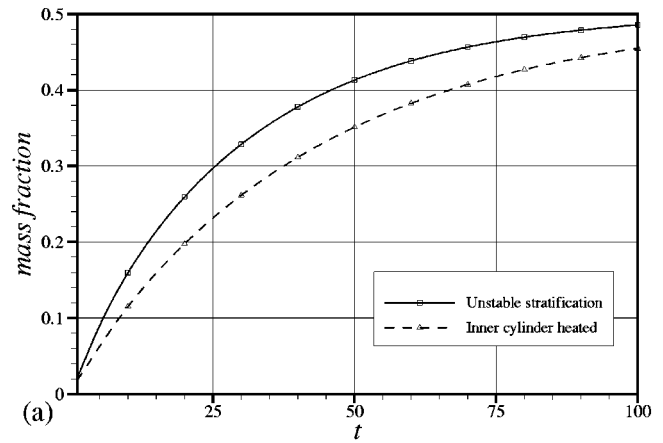


FIG. 14. Time histories of the mass fraction  $m_f$  for unstably stratified and heated inner cylinder cases.  $R_i=0.5$ . (a)  $Gr=10^3$ , (b)  $Gr=10^4$ .

13) are always more intensive than their counterparts developing when one of the cylinders is uniformly heated.

The enhancement of the mass transfer due to the unstably stratified configuration as compared to the case of the heated inner cylinder is illustrated in Fig. 14. The difference between the two cases is the largest within the time interval  $25 < t < 50$  and diminishes at  $t > 50$ . The largest difference in the mass fraction diffused into fluid 2 is about 20%.

In the present case at two fixed values of time  $t=25$  and  $50$  the diffused mass fraction  $m_f$  scales as  $Gr^\alpha$  with  $\alpha = \frac{1}{3}$  for  $50 < Gr < 10^3$  and  $\alpha \approx \frac{1}{30}$  for  $Gr > 10^4$ .

#### IV. CONCLUSIONS

In the present work we propose to use secondary natural convective flows in novel bioseparators for protein extraction. A detailed fluid mechanical analysis in the present work demonstrates that the idea is feasible, and that such a device could be competitive with the other novel bioseparators under the appropriate conditions. In particular, two-fluid natural convective flow in a horizontal cylindrical annulus and its effect on the mass transfer through the liquid-liquid interface are studied, and the flow patterns are reported. It is shown that countercurrent flow develops near the interface in contrast to most of the previously studied cocurrent cases. At large Grashof numbers the flow velocity scales as  $Gr^{1/2}$ .

The considered convective flow can be an effective tool for enhancement of the mass transfer through a liquid-liquid interface, especially in cases where the Schmidt number is large (e.g., for  $Sc \sim 10^3$ , as for proteins). It is emphasized that a natural-convection-based bioseparator/bioreactor does not contain any moving boundaries and the flow inside it can be supported for indefinite time, nor it does require too large temperature differences.

At temperature differences of the order of  $1-10^\circ\text{C}$  the present device is less effective than those employing the Taylor-Couette or the Dean vortices.<sup>1-3,22</sup> However, at the temperature difference of  $50^\circ\text{C}$  the natural-convection-based bioseparator becomes competitive with the Taylor-Couette apparatus. On the other hand, the present device can provide a stronger secondary flow than the dc streaming flows due to capillary waves discussed in Refs. 4 and 23. Nevertheless, in the case of the secondary flows in emulsions<sup>4</sup> the overall mass transfer can be higher than in the present natural-convection-based device due to a much higher interfacial area in emulsions.

Variation of the radii ratio of the annulus reveals two competitive factors affecting the mass transfer through the interface. The liquid-liquid interfacial area increases as the radii ratio decreases. Consequently, the mass transfer rate tends to increase due to this factor. On the other hand, the average temperature gradient decreases together with the decrease of the radii ratio, which leads to a slow down of the convective motion. Consequently, the convective mixing of the admixture weakens, which tends to slow down the mass transfer. The competition of the two above-mentioned factors determines the overall effect of the radii ratio. No significant difference in the mass transfer rates in the cases where the inner or the outer cylinder is heated was found. It was shown that alteration of the temperature profile at the cylindrical boundaries allows for an additional heat transfer enhancement.

Study of the scaling law for the diffused mass fraction versus the Grashof number showed that the scaling is different for the intermediate ( $50 < Gr < 10^3$ ) and large ( $Gr > 10^4$ ) Grashof numbers. Depending on the boundary conditions, the diffused mass fraction scales as  $Gr^\alpha$ , where  $\frac{1}{3} < \alpha < \frac{1}{4}$  for the intermediate and  $\alpha < \frac{1}{9}$  for large Grashof numbers. This demonstrates saturation of the capability to enhance mass transfer by increasing the temperature difference beyond a certain level.

At times  $t \leq t_m$  with  $t_m = 25$  for  $Gr = 100$  and with  $t_m = 5$  for  $Gr = 10^3$  ( $R_i = 0.1$  in both cases) the transient effects in the interfacial mass transfer process are already rather small. On the other hand, the bulk mixing effects are still not too large and the concentrations far from the interface are still not changed. These two facts allow an analytical boundary layer approach for the mass transfer calculations, which resemble fairly well the fully numerical results at  $t$  close enough to  $t = t_m$ .

All the above-mentioned results are unique, and demonstrate feasibility of novel bioseparators based on natural convective flows.

## ACKNOWLEDGMENTS

This research was supported by BSF (US-Israel Binational Science Foundation) Grant No 97-118 and the Israel High Performance Computer Unit.

- <sup>1</sup>G. Baier, M. D. Graham, and E. N. Lightfoot, "Mass transport in a novel two-fluid vortex extractor," *AIChE J.* **46**, 2395 (2000).
- <sup>2</sup>G. Baier, T. M. Grateful, M. D. Graham, and E. N. Lightfoot, "Prediction of mass transfer rates in spatially periodic flows," *Chem. Eng. Sci.* **54**, 343 (1999).
- <sup>3</sup>A. L. Yarin, A. Yu. Gelfgat, and P. Z. Bar-Yoseph, "Enhancement of mass transfer in a two-layer Taylor-Couette apparatus with axial flow," *Int. J. Heat Mass Transf.* **45**, 555 (2002).
- <sup>4</sup>A. L. Yarin, "Stationary d.c. streaming due to shape oscillations of a droplet and its effect on mass transfer in liquid-liquid systems," *J. Fluid Mech.* **444**, 321 (2001).
- <sup>5</sup>A. Yu. Gelfgat, A. L. Yarin, and P. Z. Bar-Yoseph, "Three-dimensional instability of a two-layer Dean flow," *Phys. Fluids* **13**, 3185 (2001).
- <sup>6</sup>L. R. Mack and E. H. Bishop, "Natural convection between horizontal concentric cylinders for low Rayleigh numbers," *Q. J. Mech. Appl. Math.* **21**, 223 (1968).
- <sup>7</sup>T. H. Kuehn and R. J. Goldstein, "An experimental and theoretical study of natural convection in the annulus between horizontal concentric cylinders," *J. Fluid Mech.* **74**, 695 (1976).
- <sup>8</sup>P. M. Kolesnikov and V. I. Bubnovich, "Non-stationary conjugate free-convective heat transfer in horizontal cylindrical coaxial channels," *Int. J. Heat Mass Transf.* **31**, 1149 (1988).
- <sup>9</sup>K. Vafai and C. P. Desai, "Comparative analysis of the finite-element and finite-difference methods for simulation of buoyancy-induced flow and heat transfer in closed and open ended annular cavities," *Numer. Heat Transfer, Part A* **23**, 35 (1993).
- <sup>10</sup>J. D. Chung, C.-J. Kim, H. Yoo, and J. S. Lee, "Numerical investigation on the bifurcative natural convection in a horizontal concentric annulus," *Numer. Heat Transfer, Part A* **36**, 291 (1999).
- <sup>11</sup>J. Mizushima, S. Hayashi, and T. Adachi, "Transitions of natural convection in a horizontal annulus," *Int. J. Heat Mass Transf.* **44**, 1249 (2001).
- <sup>12</sup>M. P. Dyko, K. Vafai, and A. K. Mojtabi, "A numerical and experimental investigation of stability of natural convective flows within a horizontal annulus," *J. Fluid Mech.* **381**, 27 (1999).
- <sup>13</sup>J.-S. Yoo and S.-M. Han, "Transitions and chaos in natural convection of a fluid with  $Pr = 0.1$  in a horizontal annulus," *Fluid Dyn. Res.* **27**, 231 (2000).
- <sup>14</sup>G. Labonia and G. Gui, "Natural convection in a horizontal cylindrical annulus: oscillatory flow and transition to chaos," *J. Fluid Mech.* **375**, 179 (1998).
- <sup>15</sup>K. Fukuda, Y. Miki, and S. Hasegawa, "Analytical and experimental study on turbulent natural convection in a horizontal annulus," *Int. J. Heat Mass Transf.* **33**, 629 (1990).
- <sup>16</sup>C. P. Desai and K. Vafai, "An investigation and comparative analysis of two- and three-dimensional turbulent natural convection in a horizontal annulus," *Int. J. Heat Mass Transf.* **37**, 2475 (1994).
- <sup>17</sup>L. W. Wang and C. C. Chou, "Experimental study of natural-convection heat and mass transfer in an annular enclosure with a cold inner cylinder," *Exp. Heat Transfer* **4**, 367 (1991).
- <sup>18</sup>J. Dosch and H. Beer, "Numerical simulation and holographic visualization of double diffusive convection in a horizontal concentric annulus," *Int. J. Heat Mass Transf.* **35**, 1811 (1992).
- <sup>19</sup>A. Yu. Gelfgat, P. Z. Bar-Yoseph, and A. Solan, "Stability of confined swirling flow with and without vortex breakdown," *J. Fluid Mech.* **311**, 1 (1996).
- <sup>20</sup>A. Yu. Gelfgat, P. Z. Bar-Yoseph, and A. Solan, "Vortex breakdown and instability of swirling flow in a cylinder with rotating top and bottom," *Phys. Fluids* **8**, 2614 (1996).
- <sup>21</sup>P. B. Rhines and W. R. Young, "How rapidly is a passive scalar mixed within closed streamlines?" *J. Fluid Mech.* **133**, 133 (1983).
- <sup>22</sup>A. Yu. Gelfgat, A. L. Yarin, and P. Z. Bar-Yoseph, "Dean vortices-induced enhancement of mass transfer through an interface separating two immiscible liquids," *Phys. Fluids* **15**, 330 (2003).
- <sup>23</sup>A. L. Yarin, "Steady streaming and mass transfer due to capillary waves in a two-layer system," *Fluid Dyn. Res.* **31**, 79 (2002).
- <sup>24</sup>A. Acrivos, "Solution of the laminar boundary layer energy equation at high Prandtl numbers," *Phys. Fluids* **3**, 657 (1960).